PERGAMON

International Journal of Heat and Mass Transfer 45 (2002) 4781–4792

International Journal of HEAT and MASS TRANSFER

www.elsevier.com/locate/ijhmt

Effect of carbon-fiber brushes on conductive heat transfer in phase change materials

Jun Fukai *, Yuichi Hamada, Yoshio Morozumi, Osamu Miyatake

Department of Chemical Engineering, Kyushu University, 6-10-1, Hakozaki, Higashi-ku, Fukuoka 812-8581, Japan

Received 23 February 2002; received in revised form 9 May 2002

Abstract

Brushes made of carbon fibers are used to improve the thermal conductivities of phase change materials packed around heat transfer tubes. The transient thermal responses measured in brush/*n*-octadecane composites essentially improve as the volume fraction of the fibers and the brush diameter increase. However, there is a critical diameter above which further improvement is not expected due to thermal resistance between the fibers and the tube surface. A two-dimensional heat transfer model describing anisotropic heat flow in the composite is numerically solved. The calculated transient temperatures agree well with the experimental. A simple model is also developed to predict the heat exchange rate between the composite and the heat transfer fluid. The values of the correction factors are identified on the basis of the results for the anisotropic model.

Keywords: Conductive heat transfer; Thermal energy storage; Thermal conductivity enhancement; Carbon fiber; Heat exchanger

1. Introduction

Many phase change materials (PCMs) have been proposed as thermal energy storage materials because of their superior energy storage capacities [1,2]. However, the thermal conductivities of most PCMs are too low to provide a required heat exchange rate between the PCM and the heat transfer fluid. In this case, the thermal conductivities have to be enhanced to efficiently use the thermal energy stored in the PCM.

The thermal energy storage units are roughly divided into two types. One is a capsule type, while the other is a shell-and-tube type. As enhancement techniques for the capsule type, metal fins [3–7] and honeycombs/PCM composites [3,8,9] were frequently examined. Metal thin strips [3,9], thin walled rings [7], porous metals [10], porous graphite matrices [11], copper chips [12], porous metal foam matrices [13] and carbon fibers [14,15] were also applied to the capsule type. On the other hand, the techniques for the shell-and-tube type are limited to fins [3,16–19] and honeycombs [3,8,9,20]. It might not be easy to apply the other methods as mentioned above because the tubes arranged on the shell side prevent inserting porous materials or uniformly distributing fibers/chips on the shell side. However, it is important to propose effective methods for the shell-and-tube type for further development of the thermal energy storage units using PCMs.

When the thermal conductivity of a PCM is improved, it is important not only to increase it to a required value but also to avoid unnecessary reduction in the energy storage capacity. The volume fractions of the promoter materials in the past experimental studies were 1–2 vol.% for metal thin strips [3,9], 20 vol.% for thin walled rings [7], 60 vol.% for porous metals [10], 10–60 vol.% for porous graphite matrices [11,20], 70 vol.% for copper chips [12] and 2–10 vol.% for porous metal foam matrices [13]. The fins and honeycombs usually occupy a space of 5–10 vol.% on the shell side. In summary, the volume fractions of the promoter materials in the past studies are above a few percent.

Fukai et al. [21] developed brushes made of carbon fibers. The feature of this method is that the volume

* Corresponding author. Tel.: +81-92-642-3515; fax: +81-92-642-3519.

E-mail address: jfukai@chem-eng.kyushu-u.ac.jp (J. Fukai).

0017-9310/02/$ - see front matter
PII: S0017-9310(02)00179-5

Nomenclature

a_1, a_2	correction factor
Bi	Biot number, $h_h l_{tp}/k_m$
c_p	specific heat (J/kg K)
d_b	diameter of brush
d_i	inner diameter of tube (m)
d_v	diameter of container (m)
h	heat transfer coefficient (W/m^2 K)
k	thermal conductivity (W/m K)
$\boldsymbol{k}$	thermal conductivity tensor (W/m K)
l_1, l_2, l_3	distance between thermocouples (m)
l_{tp}	tube pitch (m)
l_{tw}	distance between tubes, $l_{tp} - d_i - 2\delta$ (m)
M	mass (kg)
n	the number of grid
Q	heat exchange rate per unit length (W/m)
Q_{max}	maximum heat exchange rate per unit length, $h_h \pi d_i (T_{h,in} - T_0)$ (W/m)
r	radial distance (m)
t	time (s)
T	temperature (K)
x, y	x- and y-coordinates (m)
X_f	local volume fraction of fibers
X_{fa}	volume ratio of fibers to brush of the diameter l_{tp}
X_{tot}	volume ratio of fibers to the composite

Greek symbols

α	thermal diffusivity, $k/c_p\rho$ (m^2/s)
δ	thickness of tube wall (m)
Φ	normalized heat exchange rate per unit length, Q/Q_{max}
ρ	density (kg/m^3)
θ	angle (rad)
Θ	dimensionless temperature, $(T - T_0)/(T_{h,in} - T_0)$
τ	dimensionless time, $\alpha_m t/l_{tp}^2$
ξ	coordinate normal to the boundary surface (m)
ζ	coordinate tangential to the boundary surface (m)

Subscripts

0	initial
in	inlet
c	composite
cal	calculation
detail	detailed model
eff	effective
exp	experiment
f	fiber
h	heat transfer fluid
iso	isotropic model
m	phase change material
p	parallel model
r	random model
s	series model
simple	simple model
t	tube

fraction of the fibers is accurately and easily controlled and that the fibers with a low volume fraction (<1 vol.%) are entirely dispersed in the PCMs. They used the brushes to improve the thermal responses in the PCMs packed into cylindrical capsules and experimentally demonstrated that the effective thermal conductivities of the fiber/PCM composites reach the maximum values theoretically predicted [21].

In this study, we propose that the carbon-fiber brushes are arranged along the tubes (Fig. 1(a)) as an enhancement technique for the shell-and-tube type. The purpose of this study is to investigate the fundamental

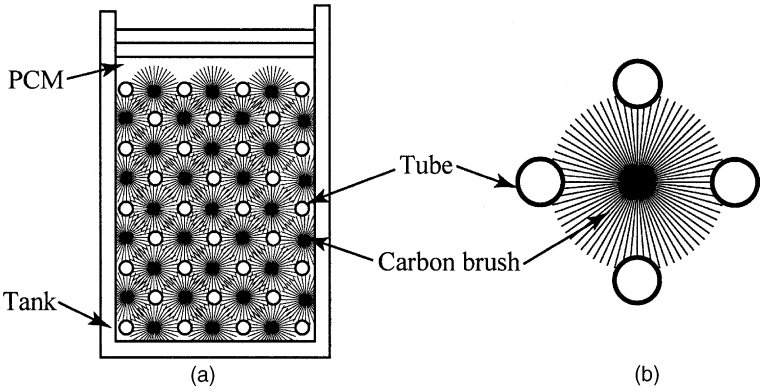

Fig. 1. Thermal energy storage units where brushes made of carbon fibers are inserted.

thermal characteristics of the brush/PCM composite surrounded by four tubes (Fig. 1(b)). The experimental apparatus imitates heat exchangers with a square arrangement. The transient thermal responses in the composite are experimentally measured to discuss the effect of the brush diameter on the heat transfer rate. A heat transfer model describing anisotropic heat flow in the composite is numerically solved. From a comparison between the experiments and the calculations, the heat transport phenomena in the composite are discussed. A simple model is moreover proposed to predict the heat exchange rate between the composite and the heat transfer fluid in the tubes. Last, the effective thermal conductivity of the composite is numerically discussed.

2. Thermal characteristics of the composite

2.1. Experimental procedure

Fig. 2(a) shows the experimental apparatus. Four steel tubes are vertically arranged in a cylindrical container made of acrylic resin. A carbon brush of 60 mm length is inserted in the center of the container. The diameters of the carbon fibers are 10 μm. The container is filled with *n*-octadecane up to a height of about 50 mm. The container is insulated using glass wool. Two to three pieces of the apparatus are prepared to examine the reproducibility of the experimental results.

Small and large apparatuses are prepared. Table 1 shows the dimensions of the apparatuses and the locations of the thermocouples in Fig. 2(b). The small apparatus corresponds to a laboratory-scale heat exchanger, while the other corresponds to a practical-scale one.

First, the apparatus was placed in a room at 18 °C overnight to maintain the container at a uniform temperature. Next, water at 23 °C was provided from a thermostatic bath to the tubes. The flow velocities of water are 0.35 m/s for the large apparatus and 0.31 m/s for the small apparatus. The transient thermal responses in the brush/PCM composite were measured. It should be noted that the experimental temperature range was below the melting point of *n*-octadecane (28 °C) to investigate the conductive heat transfer excluding latent heat.

The fiber density in the azimuthal direction is characterized by the volume fractions of the fibers to the brush of the diameter l_{tp}:

$$X_{fa} = \frac{M_f/\rho_f}{\pi l_{tp}^2/4} \tag{1}$$

where M_f is the mass of the fibers per unit longitudinal length, and ρ_f the density of the fibers. The volume

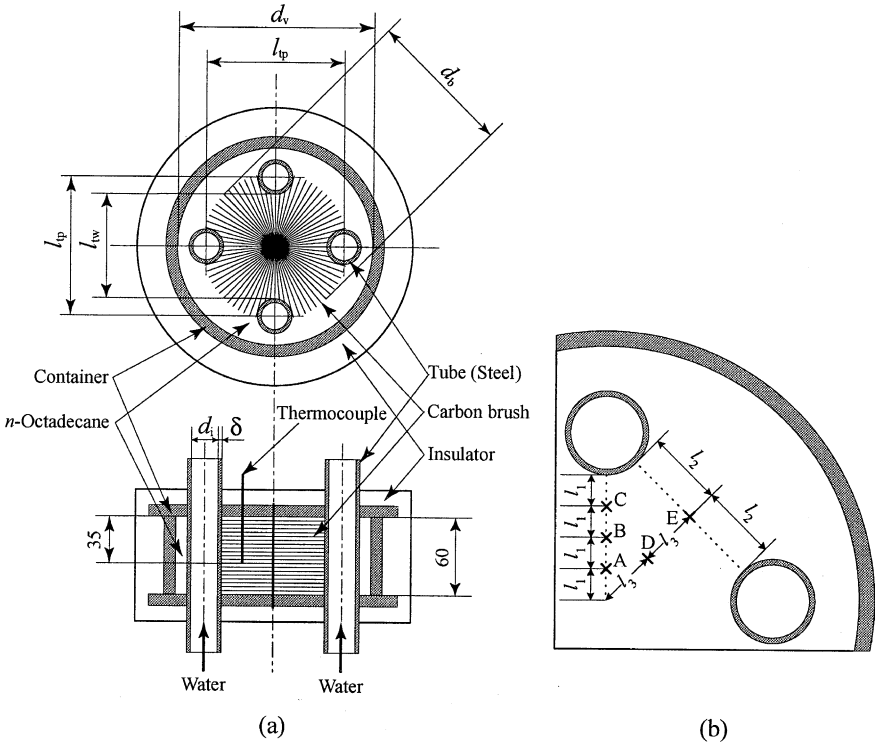

Fig. 2. Experimental apparatus and locations of thermocouples.

Table 1
Experimental apparatuses

	Dimensions of apparatuses					Locations of thermocouples		
	l_{tp}	l_{tw}	d_v	d_i	δ	l_1	l_2	l_3
Large apparatus	108.0	80.8	164	23.6	1.8	10.1	24.6	19.1
Small apparatus	36.0	26.5	56	8.0	0.75	3.3	8.0	6.4

fraction of the fibers for an arbitrary diameter was determined such that the fiber density in the azimuthal direction agrees with that of the brush for the diameter l_{tp}. Thus, the volume fraction X'_{fa} for the diameter d_b is given by

$$X'_{fa} = X_{fa}\frac{l_{tp}}{d_b} \tag{2}$$

2.2. Mathematical model

Fig. 3 shows the computational domain, which consists of the brush/PCM composite and the tube wall. Consider that the composite, including the PCM at the periphery, and tube wall are initially kept at a temperature T_0 and the fluid at a temperature $T_{h,in}$ flows in the tubes at $t > 0$. The two-dimensional conduction equations in the composite (c) and the tube wall (t) are given by

$$c_{p,c}\rho_c\frac{\partial T_c}{\partial t} = \nabla\cdot(\boldsymbol{k}_c\cdot\nabla T_c) \tag{3}$$

$$c_{p,t}\rho_t\frac{\partial T_t}{\partial t} = \nabla\cdot(k_t\nabla T_t) \tag{4}$$

where $\boldsymbol{k}_c$ is the thermal conductivity tensor. The boundary conditions are indicated in Fig. 3. The thermophysical properties of the composite are given as functions of the local volume fraction of the fibers (X_f). The heat capacity is given by

$$c_{p,c}\rho_c = X_f c_{p,f}\rho_f + (1-X_f)c_{p,m}\rho_m \tag{5}$$

The local x'–y'-coordinate, where the x'-axis is along the fiber orientation, is introduced (Fig. 3). The effective thermal conductivities in the x'- and y'-directions are given by

$$k_p = X_f k_f + (1-X_f)k_m \tag{6}$$

$$k_s = \{X_f/k_f + (1-X_f)/k_m\}^{-1}, \tag{7}$$

respectively. As a result, the thermal conductivity tensor in Eq. (3) is given by

$$\boldsymbol{k}_c = \begin{bmatrix} k_{c,xx} & k_{c,xy} \\ k_{c,yx} & k_{c,yy} \end{bmatrix} = \begin{bmatrix} \cos\theta & -\sin\theta \\ \sin\theta & \cos\theta \end{bmatrix}^{-1}\begin{bmatrix} k_p & 0 \\ 0 & k_s \end{bmatrix}\begin{bmatrix} \cos\theta & -\sin\theta \\ \sin\theta & \cos\theta \end{bmatrix} \tag{8}$$

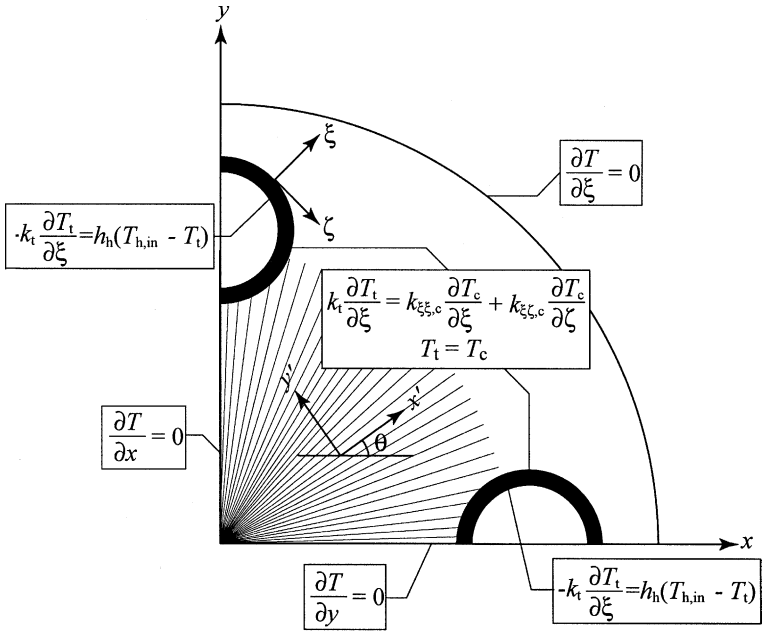

Fig. 3. Computational domain and boundary conditions corresponding to the experimental apparatus.

where θ is the angle between the x-axis and x'-axis. X_f in Eqs. (5)–(7) is approximated by the following equation [21]:

$$X_f(r) = \begin{cases} 1 & \text{at } 0 \leqslant \dfrac{2r}{l_{tp}} \leqslant \dfrac{X_{fa}}{2} \\ \dfrac{X_{fa} l_{tp}}{4r} & \text{at } \dfrac{X_{fa}}{2} < \dfrac{2r}{l_{tp}} \leqslant \dfrac{d_b}{l_{tp}} \\ 0 & \text{at } \dfrac{2r}{l_{tp}} > \dfrac{d_b}{l_{tp}} \end{cases} \quad (9)$$

where r is the radial distance from the center of the brush.

The mathematical model is numerically solved using the control volume method. The curvature surfaces are approximated using square grids. The 50×50 uniform meshes are needed to have numerical results independent of the mesh size.

2.3. Results

The properties of the materials used in the experiments are $k_m = 0.34$ W/m K, $k_f = 190$ W/m K, $k_t = 80$ W/m K, $c_{p,m}\rho_m = 1.53 \times 10^6$ J/m^3 K, $c_{p,f}\rho_f = 2.12 \times 10^6$ J/m^3 K and $c_{p,t}\rho_t = 3.48 \times 10^6$ J/m^3 K. The heat transfer coefficient h_h is nearly 1700 W/m^2 K for both apparatuses [22,23]. It is numerically confirmed that this value is so high for the estimation error of h_h that it does not affect the calculated temperature distribution in the composite. Fig. 4 shows the nondimensional time variations in the nondimensional temperatures for the large apparatus. The fiber tips do not reach the tube surface at $d_b/l_{tw} < 1$, while the fibers touch the tube surface at $d_b/l_{tw} \geqslant 1$. The curves for $d_b/l_{tw} = 0$ indicate the results for no brush. From the experiments in the figure, the transient thermal responses in the composite become sensitive as the brush diameter increases up to $d_b/l_{tw} = 1$. However, there are no remarkable differences among the experimental results for $d_b/l_{tw} \geqslant 1$. On the other hand, the calculated thermal responses improve as d_b/l_{tw} increases up to $d_b/l_{tw} = 1.11$. From the comparison between the experiments and the calculations, the model predicts well the experimental results for $d_b/l_{tw} < 1$. The brushes for $d_b/l_{tw} \geqslant 1.11$ obviously degrades the calculated thermal responses. This is because the region with high thermal conductivities is extended. This tendency is found in the experimental results for $d_b/l_{tw} \geqslant 1.11$. Fig. 5 compares the calculations to the experiments at some measurement points under various experimental conditions. The results for two pieces of the apparatus are plotted in each figure to show the reproducibility of the experiment. The calculations for $d_b/l_{tw} > 1$ certainly have errors to some degree at the points except for point E, while the model predicts well the experimental results at $d_b/l_{tw} < 1$ for all points.

The present model assumes no thermal contact resistance between the fibers and the tube surface. The fact

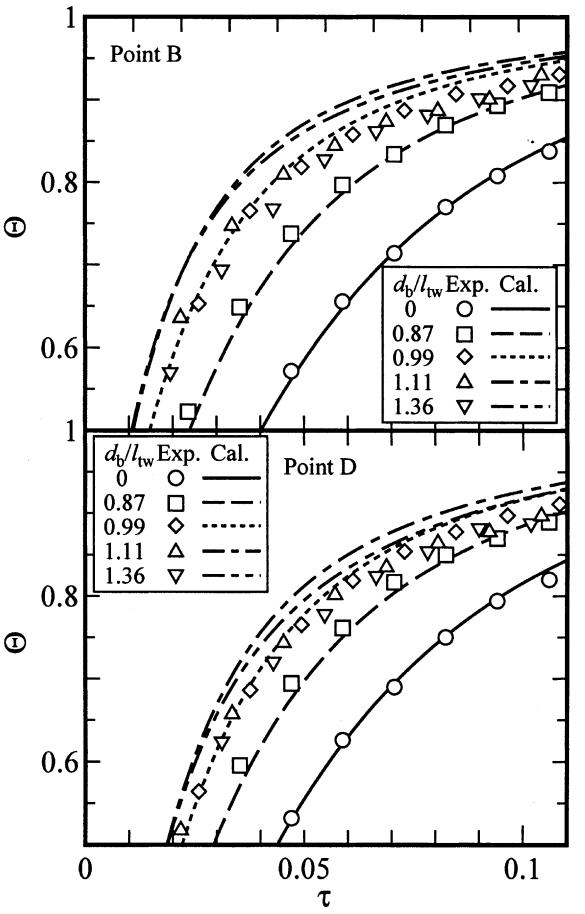

Fig. 4. The effect of the brush diameter on the transient thermal responses for the large apparatus ($X_{fa} = 0.008$).

that the experimental thermal responses for $d_b/l_{tw} > 1$ do not reach the corresponding calculations shows that there is thermal contact resistance. The thermal contact resistance might be caused by branching of the fibers near the tubes. Figs. 4 and 5 demonstrate that the thermal contact resistance affects the heat exchange rate between the composite and the fluid. At point E in Fig. 5, the calculations agree with the experiments even at $d_b/l_{tw} > 1$. This is because the fiber direction disagrees with the heat flow from the tube at point E as shown in Fig. 2, resulting in a relaxation of the overestimated heat exchange rate.

In spite of the numerical errors at $d_b/l_{tw} > 1$, Figs. 4 and 5 demonstrate that the results for $d_b/l_{tw} = 1$ approximate the experimental results for $d_b/l_{tw} > 1$. Consequently, the present model is valid for the predictions for $d_b/l_{tw} > 1$ if $d_b/l_{tw} = 1$ is assumed.

The time variation in the calculated temperature distribution in the composite under a typical condition for the large apparatus is shown in Fig. 6. When there is no

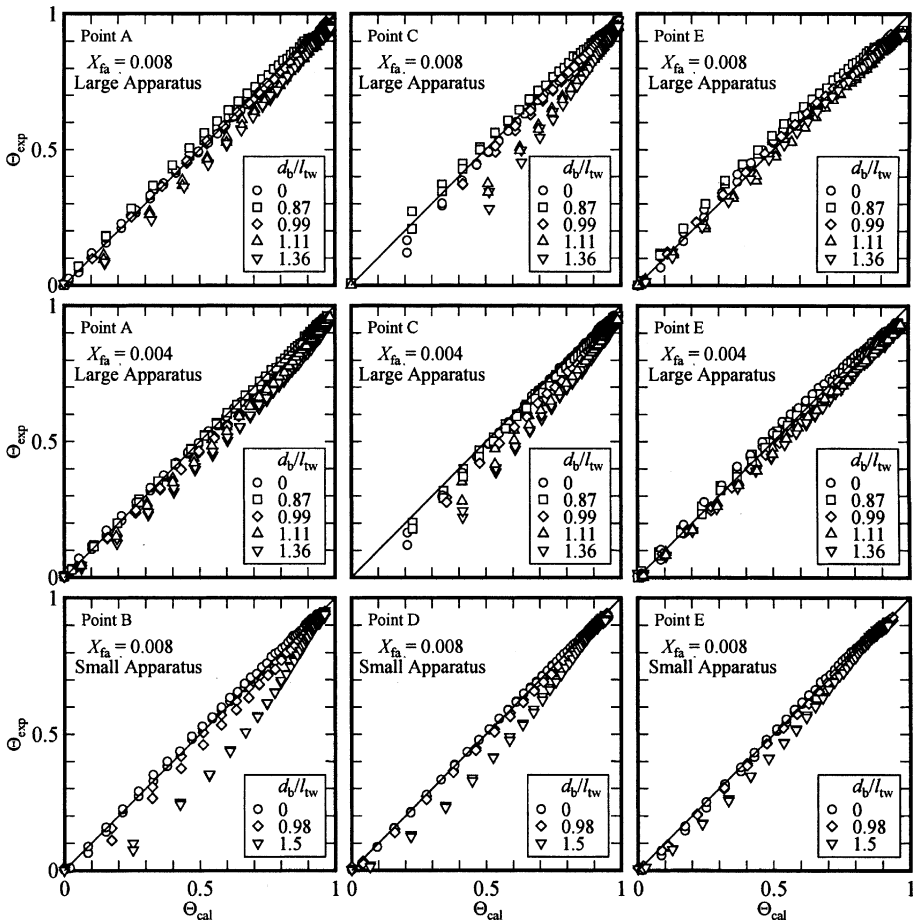

Fig. 5. Comparison between the experimental and calculated transient thermal responses.

brush ($X_{fa} = 0$), the temperature rises in a concentric configuration from the tubes, and consequently the temperature in the center region is the lowest at $\tau = 0.5$. At $X_{fa} = 0.004$ and 0.008, the heat flows preferentially from the tube surface to the center region, and the temperature in the center region rises more rapidly than that at $X_{fa} = 0$. It should be noted that the temperature in the area between the two tubes is higher than that at $X_{fa} = 0$. Although there might be thermal resistance between the fiber tips and the tube surface as mentioned above, the brush essentially enhances the thermal conductivity of PCM in the whole area surrounded with the tubes.

3. Development of a simple model

The above-mentioned model, which is referred to as a *detailed model* below, requires 200×200 meshes in a space surrounded by four tubes. Therefore, unrealistic numbers of meshes are needed when the detailed model is applied to three-dimensional heat transfer analysis in a thermal energy storage unit where there are many columns and rows of tubes. Accordingly, another model, which is referred to as a *simple model* below, is required to perform such a numerical study.

To assess the capacity of the simple model, it is necessary to compare the calculations to the experiments. However, the tube lengths of the apparatus shown in Fig. 2 are too short to calculate the heat exchange rate from the temperature difference between the inlet and outlet fluids. In addition, the apparatus does not consider the thermal contribution of the next brushes and tubes, though there are many tubes and brushes in practical thermal energy storage units as shown in Fig. 1(a). Accordingly, the detailed model is used as a reference.

The computational domain and the boundary conditions for the detailed model are shown in Fig. 7(a). The brush diameter d_b is assumed to be equal to the distance between the tubes l_{tw}.

3.1. Simplification of model

A reason for requiring many meshes in the detailed model is that straight lines approximate the curvature

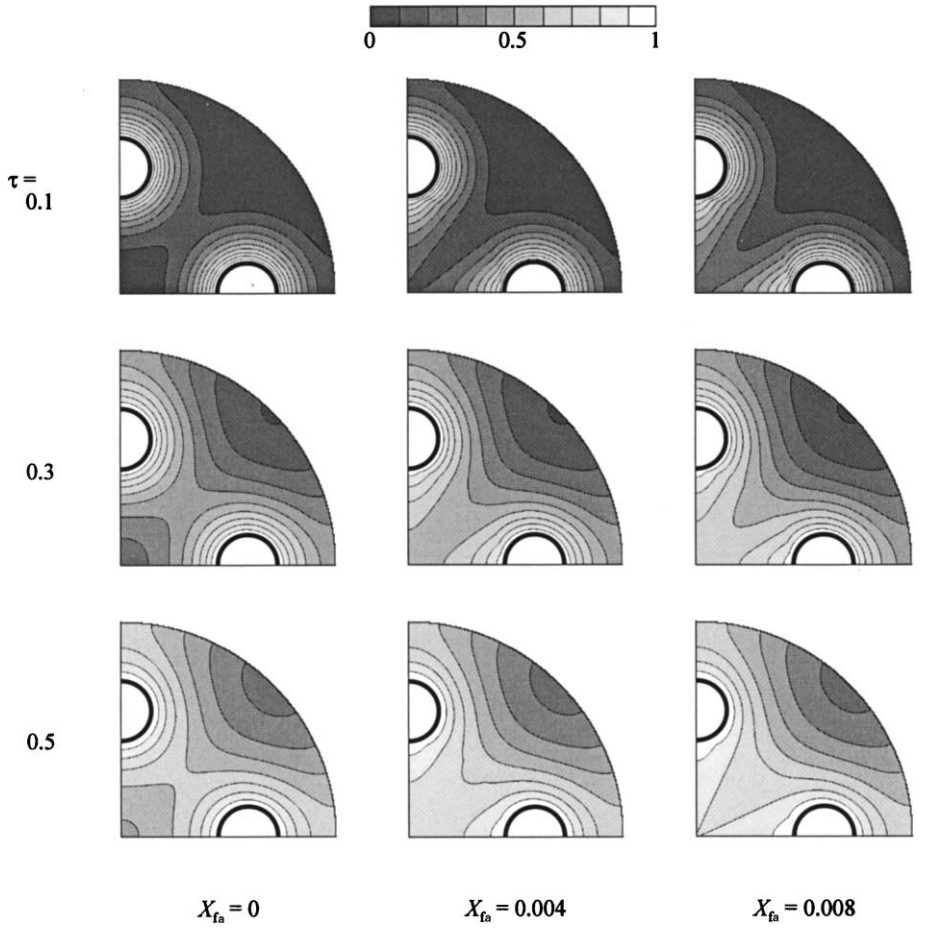

Fig. 6. The nondimensional time variation in the calculated nondimensional temperature distribution in the brush/PCM composite for the large apparatus ($d_b/l_{tw} = 1$).

surfaces of the tubes. Another is due to the anisotropic properties of the composite. Accordingly, the configuration of the tubes as well as the thermal conductivity tensor is simplified below.

The simple model corresponding to Fig. 7(a) is shown in Fig. 7(b). The circular cross-section of the tubes is assumed to be a square cross-section. The side length of the outer wall is given by $\sqrt{\pi}(d_i + 2\delta)/2$, while that of the inner wall is given by $\pi d_i/4$. Eqs. (3) and (4) are used as the governing equations. The heat capacity of the composite and the local volume fraction of the fibers are also given by Eqs. (5) and (9), respectively. To simplify the anisotropic thermal conductivity in the composite, the composite is divided into seven regions as shown in Fig. 7(b). In all regions, $k_{c,xy}$ and $k_{c,yx}$ are set to zero. In the regions A, B and C, $k_{c,xx}$ and $k_{c,yy}$ are given as the combination of the modified parallel and series models:

$$k'_p = a_1 X_f k_f + (1 - a_1 X_f) k_m \tag{10}$$

$$k'_s = [(1 - a_1) X_f / k_f + \{1 - (1 - a_1) X_f\} / k_m]^{-1} \tag{11}$$

In the region D, the fiber tips are assumed to be randomly oriented. A semi-empirical random model for chip fibers [21] is applied in this region.

$$k'_r = 0.456\{1 - (1 - a_2 X_f)^{2/3}\} k_f + (1 - a_2 X_f)^{1/3} k_m \tag{12}$$

In Eqs. (8) and (9), a_1 and a_2 are the correction factors. a_1 represents the number of the fibers contributing the heat flow from the tube surface to the center of the brush. a_2 represents the number of fibers contributing the heat flow between the tube and the composite in the region D. The components of the thermal conductivity tensor are given by

$$\text{Region A: } k_{c,xx} = k'_p, \quad k_{c,yy} = k'_p, \quad k_{c,xy} = k_{c,yx} = 0 \tag{13}$$

$$\text{Region B: } k_{c,xx} = k'_p, \quad k_{c,yy} = k'_s, \quad k_{c,xy} = k_{c,yx} = 0 \tag{14}$$

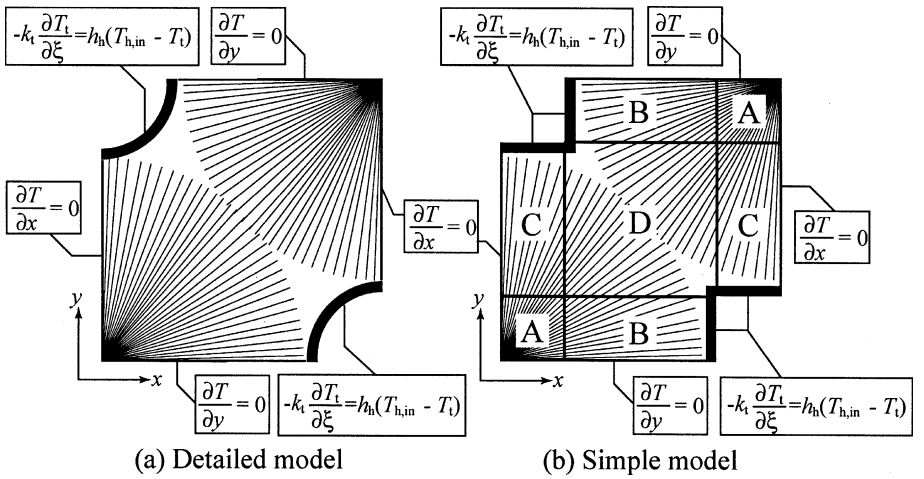

Fig. 7. Computational domain and boundary conditions corresponding to the brush/PCM composite in thermal energy storage units.

Region C: $k_{c,xx}=k'_s,\quad k_{c,yy}=k'_p,\quad k_{c,xy}=k_{c,yx}=0$ (15)

Region D: $k_{c,xx}=k'_r,\quad k_{c,yy}=k'_r,\quad k_{c,xy}=k_{c,yx}=0$ (16)

The mathematical model is numerically solved using the control volume method. The mesh size dependence of the numerical results is described in the Appendix A.

3.2. Results

The values of the correction factors in Eqs. (10)–(12) are identified through the heat exchange rate per unit length Q. First, Fig. 8 shows the normalized heat exchange rates Φ for the simple model and the detailed model at $X_{fa}=0$. Φ is defined as the ratio of Q to the maximum heat exchange rate:

$$\Phi = Q/Q_{max} = Q/\{\pi d_i h_h (T_{h,in}-T_0)\} \quad (17)$$

Apparently, the simple model predicts well the results for the detailed model. This fact shows that the simplification for the configuration of the tubes is reasonable.

The calculations were performed in the ranges $0\leqslant X_{fa}\leqslant 0.016$, $50\leqslant Bi\leqslant 5100$, $0.75\leqslant d_b/l_{tp}\leqslant 1.2$, $42\leqslant k_t/k_m\leqslant 1900$, $0.17\leqslant d_i/l_{tp}\leqslant 0.28$, $0.0033\leqslant \delta/l_{tp}\leqslant 0.017$ and $100<k_f/k_m<1500$. These ranges of the parameters

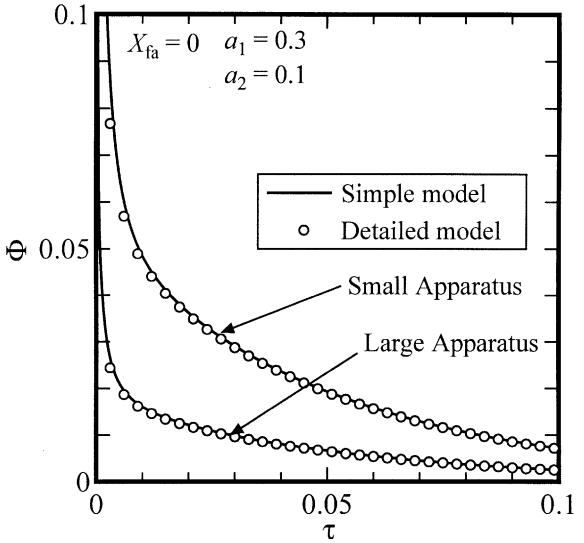

Fig. 8. The nondimensional time variations in the normalized heat exchange rates when no brush is used for the large apparatus.

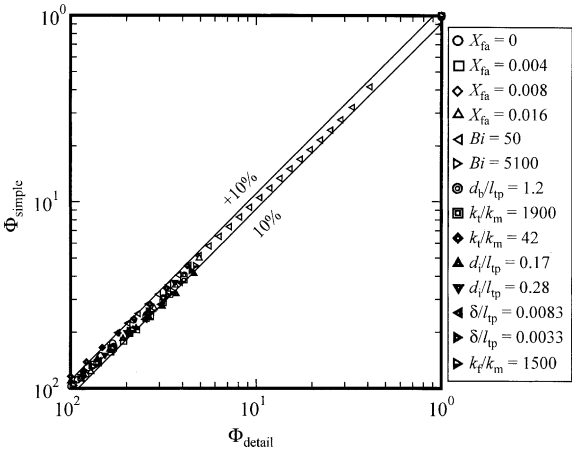

Fig. 9. Comparison between the normalized heat exchange rates calculated using the detailed and simple models. $X_{fa}=0.008$, $Bi=669$, $d_b/l_{tp}=0.75$, $k_t/k_m=412$, $d_i/l_{tp}=0.22$, $\delta/l_{tp}=0.017$ and $k_f/k_m=905$ are chosen as a base case.

probably cover the operation conditions from laboratory-scale apparatuses to practical-scale ones. The collection factors a_1 and a_2 are determined by fitting Q_{simple} to Q_{detail} using the trial-and-error technique. As a result, $a_1 = 0.3$ and $a_2 = 0.1$ are identified.

Fig. 9 shows the correlations between Φ_{simple} and Φ_{detail} during the thermal transient process. The parameter values of $X_{fa} = 0.008$, $Bi = 669$, $d_b/l_{tp} = 0.75$, $k_t/k_m = 412$, $d_i/l_{tp} = 0.22$, $\delta/l_{tp} = 0.017$ and $k_f/k_m = 905$ are chosen as a base case. This figure indicates the effects of change in various parameters. The prediction errors of the simple model are within $\pm 10\%$.

Fig. 10 compares the nondimensional temperature distributions calculated by the two models. The detailed model predicts diamond-shaped contours whose center is on the middle point between the tubes, while the simple model predicts strip contours on a diagonal line. Thus, the temperature distributions calculated using the simple model has a prediction error to some degree because the present study focuses on accurate predictions of the heat exchange rates.

4. Effective thermal conductivity of the composite

The effective thermal conductivity of the composite in the heat exchanger is estimated. To achieve it, the following isotropic heat conduction equation instead of Eq. (3) is applied to the composite region:

$$c_{p,c}\rho_c \frac{\partial T_c}{\partial t} = \nabla \cdot (k_{eff} \nabla T_c) \tag{18}$$

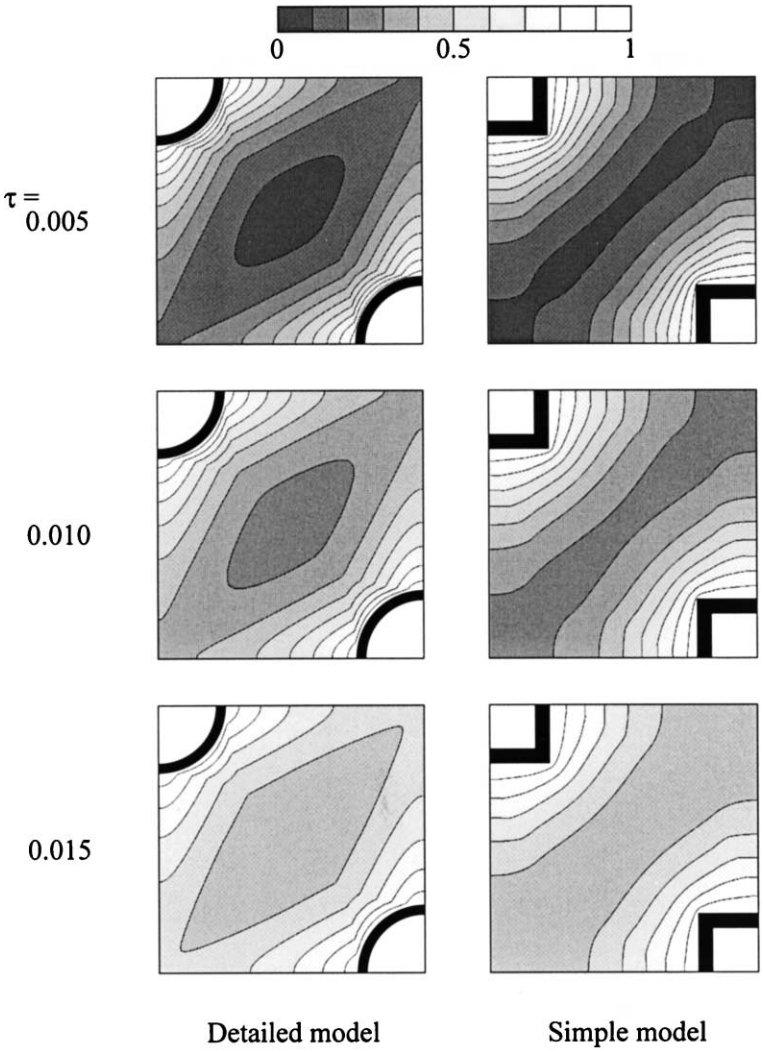

Fig. 10. The nondimensional temperature distributions calculated using the detailed and the simple models ($X_{fa} = 0.008$, $Bi = 669$, $d_b/l_{tp} = 0.75$, $k_t/k_m = 412$, $d_i/l_{tp} = 0.22$, $\delta/l_{tp} = 0.017$, $k_f/k_m = 905$).

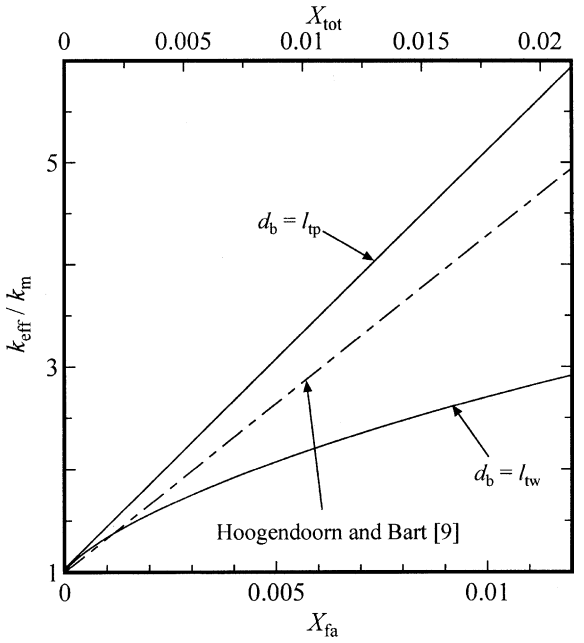

Fig. 11. The effect of the fiber volume fraction on the effective thermal conductivity ($Bi = 669$, $k_t/k_m = 412$, $d_i/l_{tp} = 0.22$, $\delta/l_{tp} = 0.017$, $k_f/k_m = 905$).

where k_{eff} is the effective thermal conductivity. This model is referred to as an *isotropic model*. On the calculation domain shown in Fig. 7(a), the time variations in the heat exchange rates Q_{detail} and Q_{iso} are calculated using the detailed and isotropic models, respectively. The value of k_{eff} is determined by fitting Q_{iso} to Q_{detail}.

Fig. 11 shows the estimated effective thermal conductivity, which is normalized using the thermal conductivity of PCM. The result for $d_b = l_{tw}$ shows the case of existing the thermal resistance near the tube wall. k_{eff} increases as X_{fa} increases. k_{eff} at $X_{fa} = 0.012$ becomes three times as large as the value of k_m. The result for $d_b = l_{tp}$ is a value excluding the thermal resistance. Hoogendoorn and Bart [9] examined an aluminum-thin-strip/paraffin matrix system. Their results are plotted against the volume ratio of the fibers/strip to the composite, X_{tot}. The relationship between X_{fa} and X_{tot} are given by

$$X_{tot} = \frac{(d_b/l_{tp})}{2/\pi - \{(d_i/l_{tp}) + 2(\delta/l_{tp})\}^2} X_{fa} \tag{19}$$

Their data do not include the thermal resistance on the heat transfer surface. The thermal conductivity of aluminum is close to that of the carbon fibers used here. From a comparison between their results and the present ones for $d_b = l_{tp}$ the present method is superior to their method.

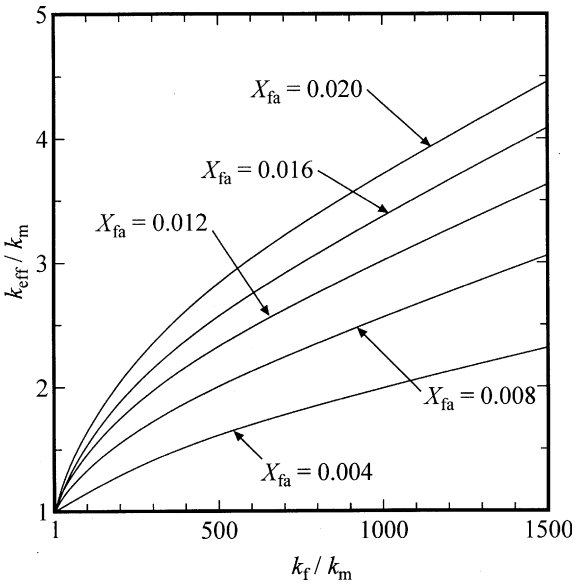

Fig. 12. The effect of the thermal conductivity ratio of fibers to PCMs on the effective thermal conductivity (d_b/l_{tw}).

Additional computation are carried out in the range $0.004 \leqslant X_{fa} \leqslant 0.020$, $50 \leqslant Bi \leqslant 5000$, $100 \leqslant k_f/k_m \leqslant 1500$, $40 \leqslant k_t/k_m \leqslant 1900$, $0.17 \leqslant d_i/l_{tp} \leqslant 0.28$, $0.0033 \leqslant \delta/l_{tp} \leqslant 0.017$. As a result, k_{eff}/k_m strongly depends on X_{fa} and k_f/k_m as shown in Fig. 12 even though it does not so much depend on the other parameters. The following equation is derived from the calculated results.

$$k_{eff}/k_m = (3.31 \times 10^{-3} + 1.69X_{fa} - 2.65 \times 10^{1}X_{fa}^2) \times (k_f/k_m - 1)^{0.67} + 1 \tag{20}$$

Eq. (20) agrees with the calculated results within $\pm 10\%$ in the aforementioned ranges.

5. Conclusion

This study experimentally and numerically investigates the fundamental thermal characteristics of the carbon-fiber brush /PCM composite. The summary is described below:

(1) The transient thermal responses in the composite improve as the diameter of the brush increases.
(2) The transient thermal responses in the composite, however, do not further improve when the diameter of the brush is larger than the distance between the tubes due to thermal resistance near the tube wall.
(3) The effective thermal conductivity, including the effect of the thermal resistance, of the composite is about three times as large as that of PCM at only $X_{fa} = 0.012$.

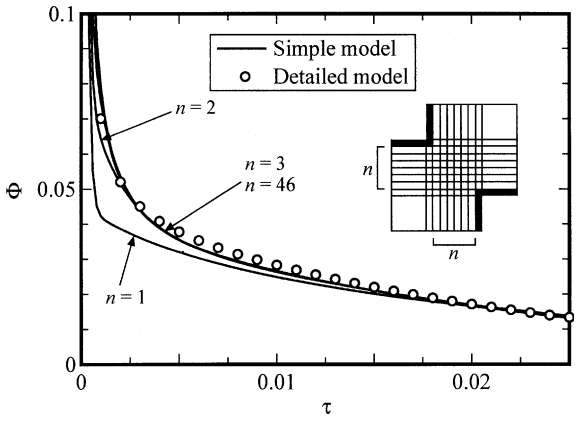

Fig. 13. Effect of mesh size on the calculated result for a base case ($X_{fa} = 0.008$, $Bi = 669$, $d_b/l_{tp} = 0.75$, $k_t/k_m = 412$, $d_i/l_{tp} = 0.22$, $\delta/l_{tp} = 0.017$, $k_f/k_m = 905$).

(4) The detailed model predicts well the experimental temperature in the composite.
(5) The simple model is developed to simulate the heat exchange rate between the heat transfer fluid and the composite.

Acknowledgements

We thank the Nippon Graphite Fiber Corporation for providing the carbon fibers.

Appendix A

The meshes are generated as shown in Fig. 13. n is the number of meshes in the x- and y-axes, respectively, in the region D in Fig. 7(b). The meshes at both ends of the region D are placed so as to fit with the thickness of the tube wall. The normalized heat exchange rate calculated using the simple model is independent of n when $n > 3$. It also agrees well with the detailed model even though large meshes are adapted into the region A. This is because the temperature gradient is not large in this region, as shown in Fig. 10. As a result, the value of $n = 5$ is chosen in the present study.

References

[1] A. Abhat, Low temperature latent heat thermal energy storage: heat storage materials, Sol. Energy 30 (1983) 313–332.
[2] S.M. Hasnain, Review on sustainable thermal energy storage technologies, part I: heat storage materials and techniques, Energy Convers. Manage. 39 (1998) 1127–1138.
[3] A.G. De Jong, C.J. Hoogendoorn, Improvement of heat transport in paraffines for latent heat storage systems, Therm. Storage Sol. Energy (1981) 123–133.
[4] S.S. Al-Jandal, Experimental study of temperature dependent heat transfer during melting and solidification processes, in: Proceedings of the Second World Renewable Energy Congress of UK, 1992, pp. 1097–1105.
[5] I.M. Bugaje, Enhancing the thermal response of latent heat storage systems, Int. J. Energy Res. 21 (1997) 759–766.
[6] M. Lacroix, M. Benmadda, Numerical simulation of natural convection-dominated melting and solidification from a finned vertical wall, Numer. Heat Transfer, Part A 31 (1997) 71–86.
[7] R. Velraj, R.V. Seeniraj, B. Hafner, C. Faber, K. Schwarzer, Heat transfer enhancement in a latent heat storage system 65 (1999) 171–180.
[8] S.M. Hasnain, B.M. Gibbs, Effect of extended surfaces in a solar energy storage unit, in: Proceedings of the Second UK National Conference on Heat Transfer of UK, 1988, pp. 833–844.
[9] C.J. Hoogendoorn, G.C.J. Bart, Performance and modeling of latent heat stores, Energy 48 (1992) 53–58.
[10] J.A. Weaver, R. Viskanta, Melting of frozen, porous media contained in a horizontal or a vertical, cylindrical capsule, Int. J. Heat Mass Transfer 29 (1986) 1943–1951.
[11] X. Py, R. Olives, S. Mauran, Paraffin/porous-graphite-matrix composite as a high and constant power thermal storage material, Int. J. Heat Mass Transfer 44 (2001) 2727–2737.
[12] A.M. Tayeb, Use of some industrial wastes as energy storage media, Energy Convers. Manage. 37 (1996) 127–133.
[13] V.V. Calmidi, R.L. Mahajan, The effective thermal conductivity of high porosity fibrous metal foams, Trans. ASME 121 (1999) 466–471.
[14] J. Fukai, H. Omori, A. Oishi, O. Miyatake, Effect of carbon fibers on thermal response within heat storage material, Kagaku Kogaku Ronbun. 23 (1997) 82–87.
[15] J. Fukai, A. Oishi, Y. Kodama, M. Kanou, O. Miyatake, Improvement of discharge characteristics of latent heat thermal energy storage unit by using carbon fibers, in: Proceedings of the Fifth ASME/JSME Joint Thermal Engineering Conference of US, AJTE99-6338, 1999.
[16] K. Sasaguchi, H. Imura, H. Furusho, Heat transfer characteristics of latent heat storage unit with a finned tube, Bull. JSME 29 (1986) 2986–2992.
[17] M. Lacroix, Study of the heat transfer behavior of a latent heat thermal energy storage unit with a finned tube, Int. J. Heat Mass Transfer 36 (1993) 2083–2092.
[18] Y. Zhang, A. Faghri, Heat transfer enhancement in latent heat thermal energy storage system by using an external radial finned tube, J. Enhanc. Heat Transfer 3 (1996) 119–127.
[19] K.A.R. Ismail, C.L.F. Alves, M.S. Modesto, Numerical and experimental study on the solidification of PCM around a vertical axially finned isothermal cylinder, Appl. Therm. Eng. 21 (2001) 53–77.
[20] O. Nomura, K. Tanaka, Y. Abe, Y. Takahashi, K. Kanari, M. Kamimoto, Heat transfer experiments on latent

thermal storage units using composite materials for space solar dynamic power systems, Space Power 12 (1993) 229–253.

[21] J. Fukai, M. Kanou, Y. Kodama, O. Miyatake, Thermal conductivity enhancement of energy storage media using carbon fibers, Energy Convers. Manage. 41 (2000) 1543–1556.

[22] B.S. Petukhov, Heat transfer and friction in turbulent pipe flow with variable physical properties, Adv. Heat Transfer 6 (1970) 503–564.

[23] V. Gnielinski, New equations for heat and mass transfer in turbulent pipe and channels flow, Int. Chem. Eng. 16 (1976) 359–368.